

## Numerical simulation of Martian dust devils

Anthony D. Toigo

Center for Radiophysics and Space Research, Cornell University, Ithaca, New York, USA

Mark I. Richardson and Shawn P. Ewald

Division of Geological and Planetary Sciences, California Institute of Technology, Pasadena, California, USA

Peter J. Gierasch

Department of Astronomy, Cornell University, Ithaca, New York, USA

Received 31 October 2002; revised 12 February 2003; accepted 17 March 2003; published 5 June 2003.

[1] Large eddy simulations of vertical convective vortices and dust devils in the Martian convective boundary layer are presented, employing a version of the Mars MM5 mesoscale model, adapted to use periodic boundary conditions and run at resolutions of 10 to 100 m. The effects of background horizontal wind speed and shear on dust devil development are studied in four simulations, each extending over the daytime portion of one Martian day. The general vorticity development in all cases is similar, with roughly equal positive and negative vorticity extrema. Two dust devils were found to develop in the highest wind speed case and in a case run without background wind. The dust devil structures were found to agree well qualitatively with terrestrial dust devil observations, including the prediction of greatly diminished vertical velocities in the vortex core.

Thermodynamic scaling theory of dust devils was found to provide good prediction of the relationship between central pressure and temperature in the modeled vortices.

Examination of the turbulent kinetic energy budgets suggests balance between buoyancy generation and loss through dissipation and transport. The vorticity for the dust devils is provided by twisting of horizontal vorticity into the vertical. The horizontal vorticity originates from horizontal variations in temperature at the lower boundary (thermal buoyancy). While the horizontal winds generated by the modeled dust devils were likely insufficient to lift dust, this study provides a solid starting point for dynamic modeling of what may be an important component of the Martian dust cycle.

*INDEX TERMS:* 5445  
Planetary: Solid Surface Planets: Meteorology (3346); 3307 Meteorology and Atmospheric Dynamics: Boundary layer processes; 3314 Meteorology and Atmospheric Dynamics: Convective processes; 3329 Meteorology and Atmospheric Dynamics: Mesoscale meteorology; 3337 Meteorology and Atmospheric Dynamics: Numerical modeling and data assimilation;  
*KEYWORDS:* Dust devil, atmospheric boundary layer, large eddy simulation, Mars

**Citation:** Toigo, A. D., M. I. Richardson, S. P. Ewald, and P. J. Gierasch, Numerical simulation of Martian dust devils, *J. Geophys. Res.*, 108(E6), 5047, doi:10.1029/2002JE002002, 2003.

### 1. Introduction

[2] Convective boundary layers generate a variety of dynamical structures. Dust devils provide a dramatic example of these structures due to the entrainment of dust within the walls of convective vortices. The lifting of dust does not actually appear to be of major dynamical importance for the development of these vertical vortices [Sinclair, 1969, 1973]. Instead, only a fraction of convective vortices develop into visible "dust devils", and even then, only a fraction of the vortex is populated with dust and becomes visible.

[3] Dust devils and convective vortices are commonly observed in desert areas on the Earth, and have also been observed in the Martian atmosphere from orbiting and landed spacecraft [Ryan and Lucich, 1983; Thomas and Gierasch, 1985; Schofield et al., 1997; Metzger et al., 1999; Malin and Edgett, 2001; Cantor et al., 2002; J. Fisher et al., A survey of Martian dust devil activity using Mars Global Surveyor Mars Orbiter Camera images, submitted to Journal of Geophysical Research, 2002 (hereinafter referred to as Fisher et al., submitted manuscript, 2002)]. They are of significant interest in studies of the Martian atmosphere for two main reasons. First, vertical vortices form as a part of the convective boundary layer, which is a poorly understood component of the Martian atmosphere. Their observed development provides an observational test for resolved models of the planetary boundary layer (PBL). Second,

the injection of dust into the Martian atmosphere remains a major problem for studies of the Martian atmosphere and climate [Zurek *et al.*, 1992]. Dust devils provide an observable form of dust lifting, and as such, study of their dynamics is of broader significance for study of global feedbacks between climate, circulation, and the dust on Mars.

[4] Suspended atmospheric dust is a major driver of the Martian circulation and climate [Zurek *et al.*, 1992]. While it is tempting to ascribe the seasonal cycle of dustiness to fallout from large (regional and global scale) dust storms, the observed year-to-year repeatability of Martian atmospheric temperatures and dust opacities in northern spring and summer [Liu *et al.*, 2003] suggests that it cannot be explained by large storms alone. Instead, a steady source of atmospheric dust is needed that generates a seasonal, essentially repeatable supply pattern. Dust devils have been widely suggested to operate in this role [Greeley *et al.*, 1992].

[5] Much previous study of Martian dust devils has focused on observations [Ryan and Lucich, 1983; Thomas and Gierasch, 1985; Schofield *et al.*, 1997; Metzger *et al.*, 1999; Malin and Edgett, 2001; Cantor *et al.*, 2002; Murphy and Nelli, 2002; Fisher *et al.*, submitted manuscript, 2002] or analytical modeling of dust devils as thermodynamic systems [Renno *et al.*, 1998]. More recently, numerical models at very high resolution have been used to generate vertical columnar vortices which bear a strong resemblance to observed terrestrial and Martian dust devils [Kanak *et al.*, 2000; Rafkin *et al.*, 2001]. In this paper, we use a very high resolution numerical model to examine such vertical columnar convection in detail and to compare the simulated structures with observations. In the next section, we give a brief description of the model (section 2). We then proceed to describe the thinking behind the experiments we have undertaken (section 3), before moving on to present the modeling results. We describe the occurrence (section 4) and origin (section 5) of modeled dust devils, and then describe their vertical and horizontal structure (section 6). After comparing them with thermodynamic theory and terrestrial observations (section 7), we discuss the origin of their turbulent kinetic energy and vorticity (section 8). We finally provide a summary of our major findings and conclusions (section 9).

## 2. Model Description

[6] This study uses an adapted version of the Pennsylvania State University (PSU)/National Center for Atmospheric Research (NCAR) Community Mesoscale Model (MM5). MM5 is a nonhydrostatic model that includes treatment of the full, three-dimensional Coriolis torque [Dudhia, 1993]. It has been adapted to Mars to study lander meteorology data records [Toigo and Richardson, 2002] and dust lifting by polar cap edge wind systems [Toigo *et al.*, 2002]. The Martian model (the Mars MM5) includes treatment of heating due to the solar and thermal infrared radiative interactions with atmospheric dust and CO<sub>2</sub>, injection and transport of dust and water vapor, and surface energy balance and subsurface heat diffusion [Toigo and Richardson, 2002]. All physical constants have been adjusted to appropriate Martian conditions.

[7] Two adaptations of the Mars MM5 were necessary to use the model to produce large eddy simulations (LES) for this study. LES models have sufficient spatial resolution to explicitly generate the larger portion of the PBL eddy spectrum responsible for PBL turbulent heat and momentum fluxes [Stull, 1988]. First, in order to most efficiently resolve the Martian PBL, we have implemented periodic boundary conditions (i.e., the model domain is coupled to itself across the domain walls). This modification removes the need to specify boundary conditions that cannot be directly generated from the much lower resolution GFDL Mars General Circulation Model (GCM) output (as used in earlier Mars MM5 studies) [Toigo and Richardson, 2002], and would require excessive downward nesting within the Mars MM5. The second adaptation involved the sub-grid-scale treatment of turbulent eddies. We use a modified version of the Medium Range Forecast model PBL scheme (MRFPBL) [Hong and Pan, 1996]. Since the goal of this study is to explicitly model eddies down to the limiting scale of resolution, we have sought to minimize sub-grid-scale heat and momentum mixing in the convective PBL. Thus the MRFPBL scheme was modified to produce minimum diffusion by forcing it to remain permanently in the “nighttime stable mode.” This also forces the parameterization scheme to calculate diffusivities only on the basis of local gradients. The treatment of heat and momentum exchange in the lowest model layer, which includes the surface layer, was unmodified. Above the lowest level, the diffusivities generated by the modified MRFPBL scheme are small, but not zero. If gradients of heat or momentum are large enough, sub-grid-scale diffusion can still be significant. In order to assess sensitivity, we attempted to reduce horizontal and vertical diffusivities below their calculated values, but in both cases, this yielded model numerical instabilities.

## 3. Experiments

[8] The number and nature of the experiments undertaken in this study result from a trade-off between computational resources and the scale of the dynamical features we wish to model. Computational resources constrain our domains to have at most a few hundred points in each direction. The resolution and extent of these domains is then set by the desire to resolve dust devil eddies while including at least a few anticipated thermal cells. Observed dust devils in orbiter images can be several hundred meters to over a kilometer in diameter [Malin and Edgett, 2001; Fisher *et al.*, submitted manuscript, 2002]. Extrapolating from terrestrial observations and modeling of convective cells [Willis and Deardorff, 1979; Webb, 1984; Young *et al.*, 2002], the horizontal diameter of cells was expected to be from 1 to 1.5 times the depth of the convectively mixed layer, which was expected to be roughly 4 to 5 km. Combined, these constraints suggested an initial model domain size of roughly 10 km, with horizontal resolution of 100 m. The vertical resolution was set to vary from a few tens of meters in the lower part of the domain (with the lowest level being approximately 10 m thick), to about 100 m near the top, with 57 vertical levels. The model top is located at 7.5 km.

[9] The study domain was chosen to represent a region near the Martian equator, with the surface albedo and

thermal properties being characteristic of Terra Meridiani. A single value of albedo, thermal inertia, and elevation from the Terra Meridiani region has been used (albedo = 0.16, thermal inertia =  $250 \text{ J m}^{-2} \text{ K}^{-1} \text{ s}^{-1/2}$ , elevation =  $-1400 \text{ m}$ ), and held uniform throughout the model domain (i.e., there are no spatial variations in the surface properties). The model time of year (which is important for prescribing the incident solar radiation due to the large eccentricity of Mars' orbit) was set to  $L_s = 331^\circ$  ( $L_s$  is the seasonal indicator for Mars, measured in degrees from 0 at northern spring equinox). The season and location correspond to those of a prime landing target for NASA's Mars Exploration Rovers. It is a region known to be relatively flat, and thus unlikely to be strongly perturbed by significant slope-driven wind systems. In each case, the visible dust opacity was set to a value of 0.5 and uniformly distributed with height.

[10] Four primary experiments were run, each extending over the daytime portion of the diurnal cycle, from 0930 LT (local time) to 1530 LT. (The Martian solar day is 37 minutes longer than the Earth solar day. In this paper we use a time system that is based on the Martian day, such that there are 24 "hours" or 1440 "minutes" in a Martian day. We continue to use the SI second, such that there are 61.64 s in a "minute.") At the location chosen for the simulations the Sun is up for the full duration of the model run. The runs were designed to cover local times expected to yield greatest dust devil activity (1200 to 1500 LT), and with sufficient simulation time before this to allow development of the boundary layer. The simulations were not run for a greater period for pragmatic reasons of computational cost. The simulations differ only in the initial wind distribution. In the standard ("medium wind") case, the initial wind field is derived from the GFDL Mars GCM. Variations include initial wind speeds three times faster ("high wind" case) and slower ("low wind" case), and a case with no initial wind (the "no wind" case). In the three cases with initial wind, the wind field also includes a vertical shear. These cases were run in order to assess the importance of background wind speed and shear for the development of vortices. In none of the cases do we attempt to initialize with a (geo- or cyclo-strophically) balanced state. Instead, we allow the model to adjust itself during the initial few minutes of the simulation.

#### 4. Occurrence of Dust Devils in the Large Eddy Simulations

[11] The initial wind speed and direction profiles for the four primary large eddy simulations (LESs) are shown in Figures 1a and 1b, respectively. It has been variously argued that the vorticity for dust devil development must initially be available from the horizontal mean flow of the atmosphere (see discussion by Kanak *et al.* [2000]) and that dust devils preferentially form in relatively low wind conditions [Sinclair, 1969, 1973; Ryan and Carroll, 1970] (note that hereafter, we shall use the terms "vertical vortex" and "dust devil" interchangeably, even though it is not clear whether dust would be lifted—the criteria for lifting depends on which lifting mechanisms are important for dust). The four cases provide an opportunity to test the importance of wind speed and shear, including a zero wind

case similar to that studied for terrestrial dust devils by Kanak *et al.* [2000].

[12] Ground temperature as a function of time is plotted in Figure 1c. Ground temperature varied by less than the thickness of the line among the four experiments, and the figure shows the change in energy input potentially available. The maximum and minimum values of vorticity calculated in the four primary LES domains are shown in Figure 1d as a function of local time and ground temperature (Figure 1c). The simulations show very little vertical vorticity development until just after noon. After that point, each of the simulations develop a range of vortices, with positive vorticity development (counterclockwise motion) being equally likely as negative vorticity development. The primary effect of wind appears to be to delay strong vorticity development by up to 45 minutes for the "high wind" case as compared to the "no wind" case. In each of the cases, maximum and minimum vorticities tend to very similar values by the mid-afternoon. An exception to this statement occurs in the "no wind" and "high wind" cases, corresponding in both cases to the development of dust devils. In both cases, the dust devils rotate clockwise. However, the simulations undertaken here are nearly equatorial, and thus there should be no handedness to vortex development. In any case, observations of Martian and terrestrial dust devils shows no preferred handedness in statistically significant studies well away from the equator [Ryan and Lucich, 1983; Sinclair, 1969, 1973].

[13] Figure 1d provides a very clear selection criteria for the designation of a "dust devil" event and its identification relative to the background distribution of vortical motion. The two dust devils identified in this study are centered at 1330 LT in the "high wind" case and at 1520 LT in the "no wind" case. These events are clearly discernible as they represent negative (clockwise) vorticity maxima more than twice the value of the background. This is a signal that the flow, at least in some local region, has changed its nature. Disorganized free convection is characterized by relatively small pressure and temperature perturbations [e.g., Stull, 1988]. In contrast, vortices are balanced flows in which the pressure gradient is balanced by a perpendicular centrifugal acceleration, blocking the efficient destruction of horizontal temperature contrasts. Under ideal balanced conditions, temperature contrasts are limited only by the total temperature contrast available from the lower boundary (the ground), and can be much larger than under free convection scaling.

#### 5. Description of Modeled Dust Devil Origin

[14] The development of the "no wind" case dust devil is illustrated in Figure 2. Figures 2a and 2e show the vorticity and divergence, and horizontal wind and vertical wind, respectively, at 1454 LT. At this time, several extrema of positive and negative vorticity exist in association with junctions or buckles in upwelling sheets. These sheets are components of open cellular convection generated in each of the LES experiments in this study. The vorticity extrema at this time are typical of the simulated convective boundary layer, with the extremum values falling on the envelopes of "background level" vorticity in Figure 1d.

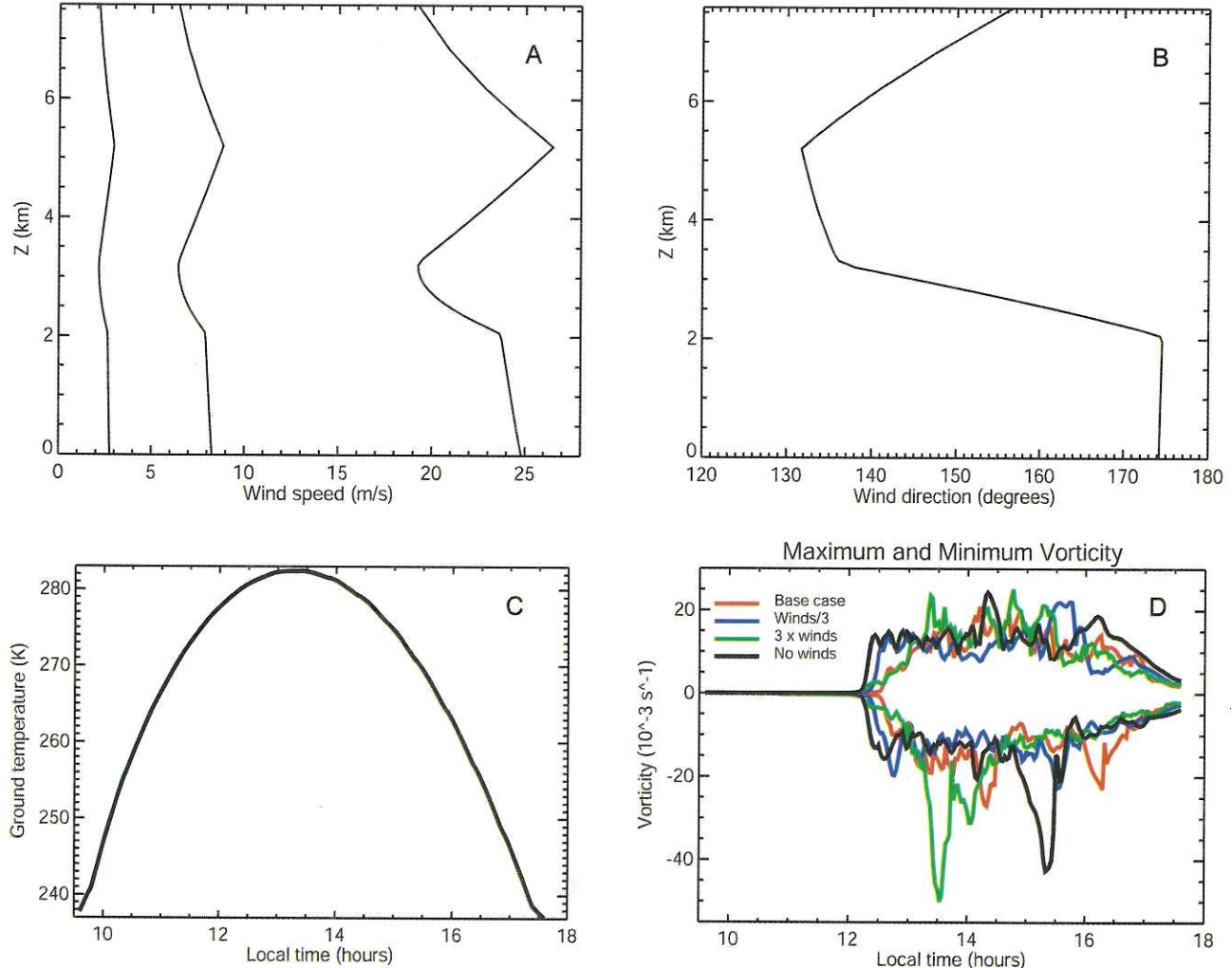


**Figure 1.** (a) Initial wind speeds as a function of height for the four simulations discussed in this study. The middle line is the “base” case. The “high wind” case was generated by taking the base profile and multiplying all wind speeds by a factor of 3. The “low wind” case was generated dividing base winds speeds by three. (b) Plot of wind direction as a function of height showing directional shear. A direction of 180 is easterly winds, and 90 is southerly. The wind direction of all four simulations was kept the same. (c) Ground temperature as a function of time from the model simulations. Differences in the ground temperature between the different simulations varied by less than a third of a Kelvin (less than the thickness of the line in the plot). Ground temperature peaks at about 1315 LT. (d) Maximum and minimum vertical vorticity in each of the four simulations as a function of time. The vertical vorticity is essentially zero until convection starts up after noon. There is little difference in the background level of vorticity between the different simulations, showing that the magnitude of the mean wind (and the vertical wind shear) do not play a large role in determining the magnitude of the vertical vorticity. The two “dust devils” stick out as large negative peaks above the background in the “no initial wind” simulation, and the “high wind” simulation.

[15] Figures 2f–2h show that the dust devil vortex develops at the intersection of several upwelling sheets. This is in agreement with ideas presented by Maxworthy [1973] and in terrestrial LES studies [Kanak *et al.*, 2000]. The horizontal wind field advects the vertical velocity sheets around the center of rotation, concentrating upwelling motion within the developing dust devil (see Figures 2f and 2g). This advection is associated with deepening of the vorticity, and circularization of the dust devil. By 1524 LT, the dust devil is very well organized and quite symmetric,

and clearly represents a very strong concentration of negative vorticity.

[16] In both cases of simulated dust devils, the vortices persist for about 45 minutes, which is in reasonable agreement with Viking Lander observations [Ryan and Lucich, 1983]. The structure and duration of the dust devils does not appear to be affected by the differences in environmental wind speeds and shear in the two LES cases. It should also be noted that while the “no wind” dust devil moves near to the model boundary, the domain

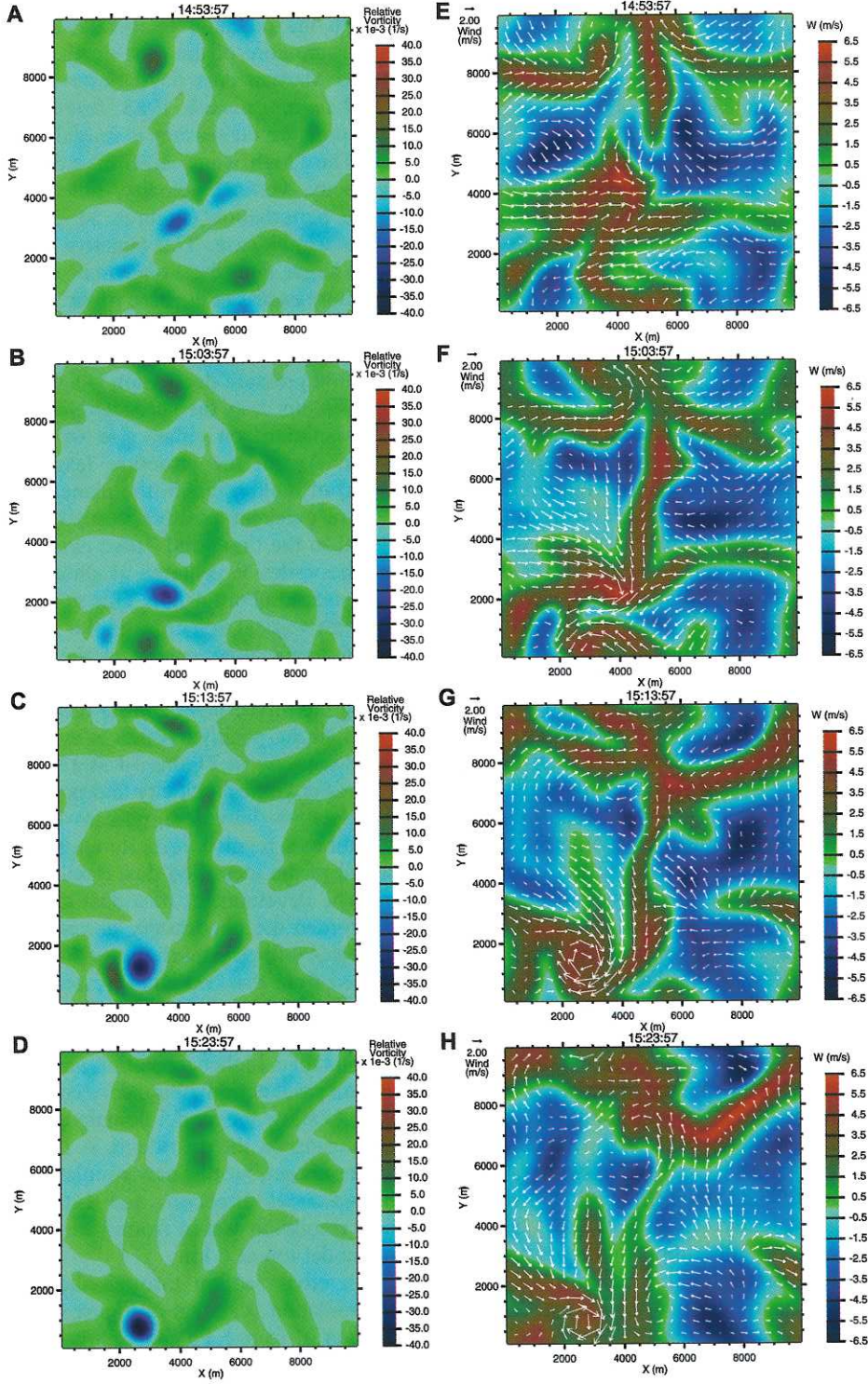


**Figure 2.** Development of the dust devil in the “no wind” simulation. Local time runs from about 1454 LT to 1524 LT. Figures 2a–2d show the magnitude of vertical vorticity at a height of about 1.4 km from the surface. Figures 2e–2h show the magnitude of the vertical wind ( $w$ ) at the same height (approximately 1.4 km above the surface) overlaid with white arrows showing the horizontal wind vector at that height. Scale bar for the wind vectors is to the left.

employs periodic boundary conditions and thus this location has no special numerical meaning (there are no edge effects).

## 6. Vertical and Horizontal Structure of Modeled Dust Devils

[17] The vertical structures of the two modeled dust devils, and that of the LES atmosphere in the same plane away from the dust devil locations, are shown in Figure 3. In both cases, the plots cross the centers of the modeled dust devils, and the time samples were chosen to coincide with maximum negative vorticity, approximately 1520 LT and 1330 LT for the “no wind” and “high wind” cases, respectively. (The plane of the cross section in Figures 3a–3d is west to east across the page in Figure 2 at the 900 m position on the y axis.)

[18] Examining the “no wind” case first, the vorticity cross section shows a very strong concentration of vorticity within the dust devil structure, which is located between the 2000 m and 3500 m positions on the x axis (Figure 3a). The total region of negative vorticity associated with the dust devil therefore has a diameter of a little less than 1.5 km. The vortex bends increasingly with height to the left of the figure. This is also the direction of motion in this plane, yielding a relationship between dust devil motion and lean that is consistent with terrestrial field observations [Sinclair, 1969, 1973]. The motion of the dust devil in this “no wind” case is due to the circulation induced by the cellular convection within which the dust devil is embedded.

[19] The dust devil height is about 4 km. The dust devil is not the only region of strong, vertically aligned vorticity. To the right of the dust devil, an counterclockwise vortex is noted that leans in the opposite direction, while the upper portion of an counterclockwise vortex is also observed above the 8000 m location. These structures correspond to the local maxima in positive vorticity just north of the cross section in Figures 2d and 2h. However, even the strong positive vortex just to the right of the dust devil has a vorticity magnitude less than 20% that of the dust devil. In addition, Figure 2 shows that circular motion does not fully develop in either of these cases.

[20] The cross section of vertical wind for the “no wind” case (Figure 3b) shows that the dust devil vortex is associated with the strongest vertical velocities at 2.5 to 3 km altitude. Above 2.5 km, the vertical velocity field is observed to split over the dust devil. We will revisit the details of the vertical velocity structure below. Strong upwelling motions occur on either side of the dust devil vortex. The rightmost of these is coincident with the weak counterclockwise vortex. Comparison with Figures 2f and 2g suggest that these secondary maxima in vertical velocity correspond to the advection and wrapping of cellular convection upwelling sheets around the dust devil central vertex by convergent winds.

[21] The potential temperature distribution provides clear indication of the buoyant drive behind the dust devil (Figure 3c). The dust devil core at lower levels is over 1 K warmer than surrounding environmental air, and similarly warmer than air at the top of the mixed layer above the dust devil. The upwelling sheets to the left and right of the dust devil are associated with much smaller potential temperature

perturbations. The potential temperature plot also suggests a mixed layer depth of roughly 5 km.

[22] The pressure perturbation (Figure 3d), in combination with the potential temperature, illustrates the warm, low-pressure core of the dust devil, consistent with terrestrial and Martian dust devil observations [Sinclair, 1969, 1973; Ryan and Lucich, 1983; Schofield et al., 1997]. The central pressure depression is roughly 1 Pa at the surface.

[23] The “high wind” LES dust devil vertical structures in vorticity, vertical velocity, potential temperature, and pressure perturbation (Figures 3e–3h) resemble those of the “no wind” case. The negative vorticity maximum is slightly larger than the “no wind” case, and the potential temperature excess at the base of the dust devil is nearer 2 K with respect to air at the top of the mixed layer (which is slightly shallower at this local time, approximately 4.5 km). The central pressure depression is again roughly 1 Pa at the surface. In this case, the vertical velocity extrema have split into two plumes on either side of the negative vorticity maxima. Again, the structure leans to the left, in the direction of motion within the plane. A somewhat stronger and more coherent positive vorticity structure than those observed in the “no wind” case exists in the “high wind” case. The vortex is centered at about the 9200 m location and extends to about 4 km. This vortex is coincident with the highest vertical velocities in the plane, and with a large potential temperature excess at the surface. This vortex, along with the identified dust devil, is responsible for buckling the mixed layer ceiling upward, as seen in Figure 3g. This strong positive vortex is evident as the maximum positive vorticity in Figure 1d at 1330 LT. Despite strong signatures in vertical velocity and potential temperature, the plume does not have a significant low-pressure core, and thus exhibits a relative vorticity magnitude of only roughly 33% that of the identified dust devil.

[24] The development of a dust devil in the “no wind” case afforded the opportunity to easily undertake a higher resolution, refined simulation of the vortex in a LES initialized from the “no wind” case. We took output from the “no wind” case for the nearly well formed vortex and used output from that LES to generate initial and boundary conditions for a higher resolution simulation. In this higher resolution case, periodic boundary conditions were not used in order to allow the model domain to be greatly reduced in size, focusing on the dust devil. A horizontal resolution of 10 m was chosen for this new simulation, with 200 points in each horizontal direction, and 140 vertical points. The vertical resolution varied from 3 m at the surface to 90 m at the model top at 6 km.

[25] A cross section through the high-resolution dust devil simulation is shown in Figure 4. The central pressure depression of over 1 Pa can clearly be seen in this figure, coinciding with an upward deflection of the air temperature surfaces, indicating a warm core. These relationships are similar to those found for terrestrial and Martian dust devils, as noted above. Figure 4 also shows that the nearly uniform vertical motion suggested in Figure 3b, actually splits into two vertical plumes when examined at high resolution. This is similar to the “high wind” case dust devil at lower resolution. This depression of vertical velocities was seen in the field data collected by Sinclair [1973], and emphasized as an important component of dust devils. These simula-

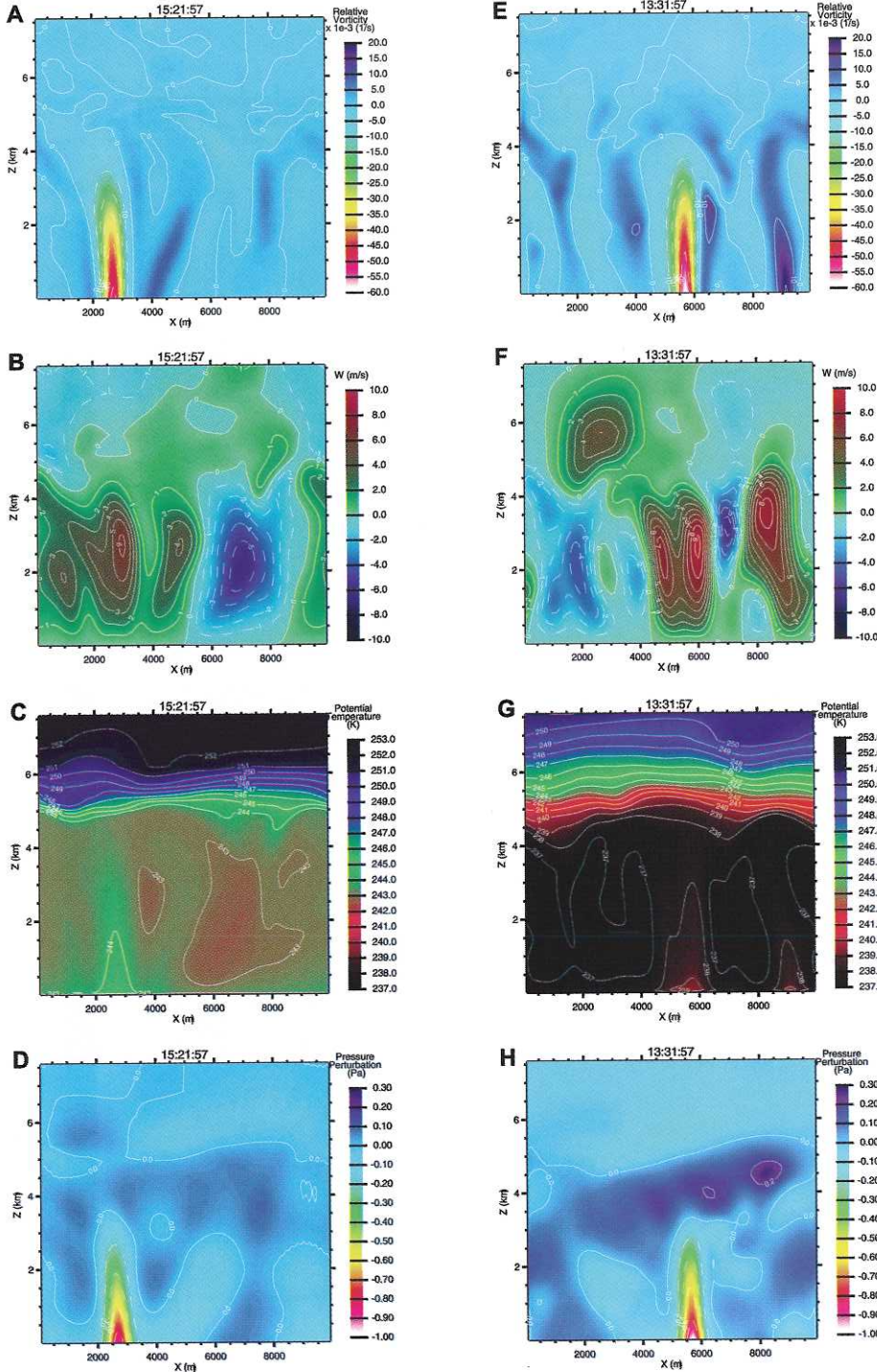


**Figure 3.** Vertical slices through the center of the two dust devils seen in our simulations. Variable values are plotted both in the color shading and in white contours. Figures 3a–3d refer to the “no wind” simulation dust devil, and Figures 3e–3h refer to the “high wind” simulation dust devil. (a) and (e) Vertical vorticity. The dust devils stand out as very large negative vorticity spikes above the background. Within the dust devils, vorticity increases (in absolute magnitude) toward the ground. (b) and (f) Vertical wind. While there are several regions of large vertical velocity seen in both plots, the dust devils represent the locations of largest vertical velocity. (c) and (g) Potential temperature. The dust devils in each simulation stand out as large positive potential temperature differences from the mean background, with the difference from background increasing toward the surface within the dust devil. (d) and (h) Pressure perturbation (difference from background pressure). The dust devils are low-pressure cells, and the magnitude of the low-pressure center is seen in these plots. The difference of pressure in the dust devil as compared to outside the dust devil is about 1 Pa, and decreases as one goes up in the dust devil.

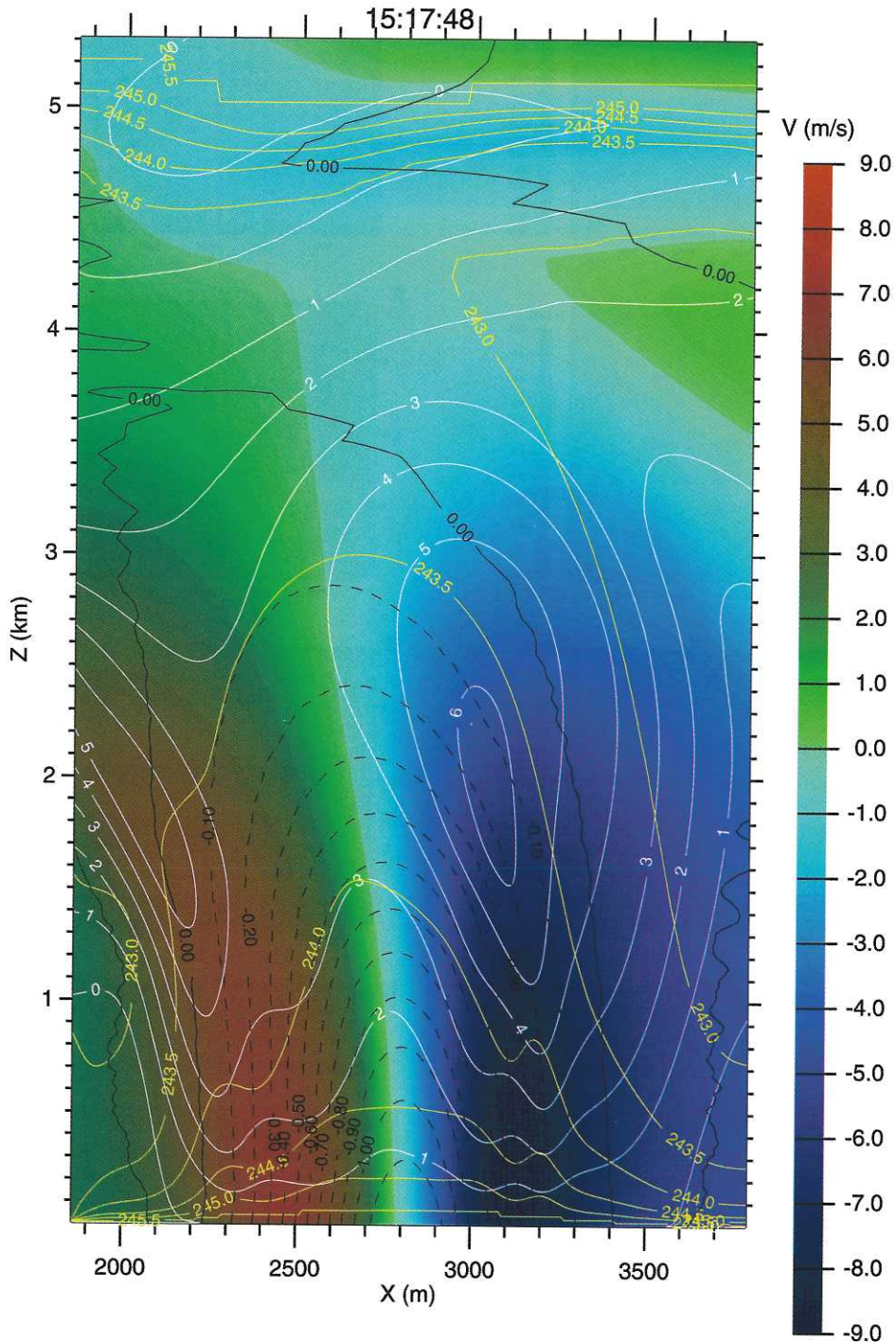


**Figure 4.** High-resolution simulation of the “no wind” simulation dust devil. A high-resolution study ( $\Delta x = 10$  m) of the dust devil seen in the “no wind” simulation was undertaken to better resolve the dust devil structure. Here is plotted a vertical slice through the center of the dust devil. Background color shows the tangential wind speed. Black contours show the pressure perturbation in Pa, still reaching a maximum difference near the surface of about 1 Pa less than the background. Yellow contours show potential temperature in K, and the warm core of the dust devil. White contours show upward wind velocity in m/s. Upward wind velocity peaks at the walls of the dust devil, and the decrease in upward velocity can be seen in the center of the dust devil core.

tions clearly show a strong depression of vertical motion in the core of the dust devils, in agreement with observations. This decrease of upward motion in the dust devil core clearly confirms the tentative identification of a vertical velocity minimum in the terrestrial LES study of *Kanak et al.* [2000]. However, it is much stronger in the dust devils reported here due to their larger size and the higher resolution of this simulation. Indeed, in the lowest few tens of meters, the high-resolution simulation shows downward motion at the core of the dust devil (not shown), in excellent agreement with the *Sinclair* [1973] observations. Tangential winds shown in Figure 4 peak at 9 m/s and 7.2 m/s on the right and left hand sides of the vortex center. The relationship between these winds, the central pressure, and central temperature values will be discussed in the next section.

[26] A more detailed picture of the horizontal structure of the “no wind” case LES dust devil is shown in Figure 5. The context for the high-resolution dust devil simulation is shown in Figure 5a. The relationship between the convection cell updraft walls and the dust devil vortex is evident in this image. At this stage, the vortex vorticity field is seen to be wrapping the updraft sheets around the vortex center, generating the secondary updraft structures commented upon in Figure 3b. Figure 5b shows the higher resolution domain. The figure shows the tight collocation of the temperature maxima, the central pressure depression, and the center of curvature of the wind field. Again, this figure shows the action of the vortex wind field in wrapping the intersecting convective cell updraft sheets to form the dust devil vortex wall.

## 7. Comparison of Modeled Dust Devils With Thermodynamic Theory and Observations

[27] Assuming that dust devil vortices are in cyclostrophic balance, the maximum tangential wind in a dust devil is independent of dust devil radius, and the relationship between the central pressure drop and the maximum tangential wind can be written directly from the cyclostrophic balance equation as

$$v = \sqrt{\frac{RT}{P} \Delta P} \quad (1)$$

where R is the gas constant, T is the mean temperature, P is the mean pressure, and  $\Delta P$  is the central pressure drop. Using values of  $T = 240$  K,  $P = 650$  Pa,  $R = 187$  J/kg/K, and  $\Delta P = 1$  Pa, we estimate a maximum tangential wind for the dust devil shown in Figure 4 of roughly 8.5 m/s. This is quite close to the modeled peak winds (approximately 8.7 m/s, after correcting for motion of the dust devil itself), and this approximation works well for observed terrestrial and Martian dust devils [*Renno et al.*, 1998, 2000; *Murphy and Nelli*, 2002].

[28] The relationship between the central pressure drop, central pressure temperature rise, and peak vertical wind speeds is less straightforward. To address these relationships, a thermodynamic theory for dust devils has been developed by *Renno et al.* [1998] and has been applied to lander-based observations of Martian dust devils [*Renno et al.*, 2000; *Murphy and Nelli*, 2002]. The scaling theory relates central pressure drop to the ambient thermal varia-

bles and to a measure of the fraction of total frictional dissipation that occurs at the surface. Using equation (24) from *Renno et al.* [1998], with the value of  $c_p = 770$  J/kg/K, the mixed layer top pressure,  $P_{top} = 460$  Pa, and a temperature increase of approximately 1.5 K at the vortex center relative to ambient, we obtain a predicted central pressure drop of about 0.7 Pa. This compares reasonably well with our modeled pressure drop of about 1 Pa. However, we generally produce a lower value of the pressure drop for a given temperature excess in the dust devil core than presented by *Renno et al.* [2000] and *Murphy and Nelli* [2002]. The main discrepancy is in the assumed depth of the convective plumes. Our model shows a plume depth and a mixed layer depth of about 5 to 6 km (Figures 3c and 3g) whereas *Renno et al.* [2000] assumed a minimum depth of one scale height, and a limiting depth of the whole troposphere, or about 45 km [Zurek et al., 1992]. In general, the Martian troposphere is quite stable due to the presence of suspended dust, yielding an environmental lapse rate of about 3 K/km compared to an adiabatic lapse rate of about 5 K/km. This stability, combined with the absence of thermodynamically significant water vapor in Martian air, limits ordinary convective plume and PBL mixed layer depths. This limit is likely only breached in cases of plumes focused over sharp topographic relief.

[29] The modeled dust devils may be compared with dust devils observed by the Mars Pathfinder (MPF) meteorology package [*Schofield et al.*, 1997; *Renno et al.*, 2000; *Murphy and Nelli*, 2002]. Both simulated dust devils developed central pressure drops of about 1 Pa. This places the modeled structures as typical, small dust devils observed by MPF (compare with *Murphy and Nelli* [2002] and Table 1 of *Renno et al.* [2000]). The local time of occurrence for the “high wind” case LES dust devil is typical of the MPF dust devils, while the “no wind” case LES dust devil occurs about an hour after the latest MPF dust devil. The MPF observations do not provide information on dust devil duration.

[30] Figure 6 shows the radial distribution of tangential wind through the high-resolution simulation of the “no wind” case dust devil. The section is at a height of 500 m and is from left to right as viewed in Figures 4 and 5. The dust devil translational speed in this direction of 1.2 m/s has been removed from the velocities plotted. Superposed on this plot are lines of  $vr = constant$  and  $v/r = constant$ . Within the vortex core (which we define as the region contained within peak tangential winds) to a radial distance of about 200 m, vortex is rotating as a solid body. Within this region,  $v/r$  is conserved. The vortex increasingly sub-rotates relative to a solid body out to the vortex wall. Beyond the vortex core, the tangential velocity structure is better defined with  $vr = constant$ . On the right hand side of the vortex, profiles of  $vr$  held to a constant defined by the speed at a radial distance of 1000 m, and with the constant defined by the value of the solid body rotation speed at the vortex wall agree very well. On the left-hand side of the vortex, the two  $vr$  curves are offset, while the shapes of the curves agree quite well with the observed decrease in wind speed away from the vortex center. The discrepancy likely results from the ellipticity of the modeled dust devil, as seen in Figure 5. Despite the modest discrepancies, the modeled dust devil appears to agree quite well with the behavior of a Rankine vortex, which has been shown to compare very well with

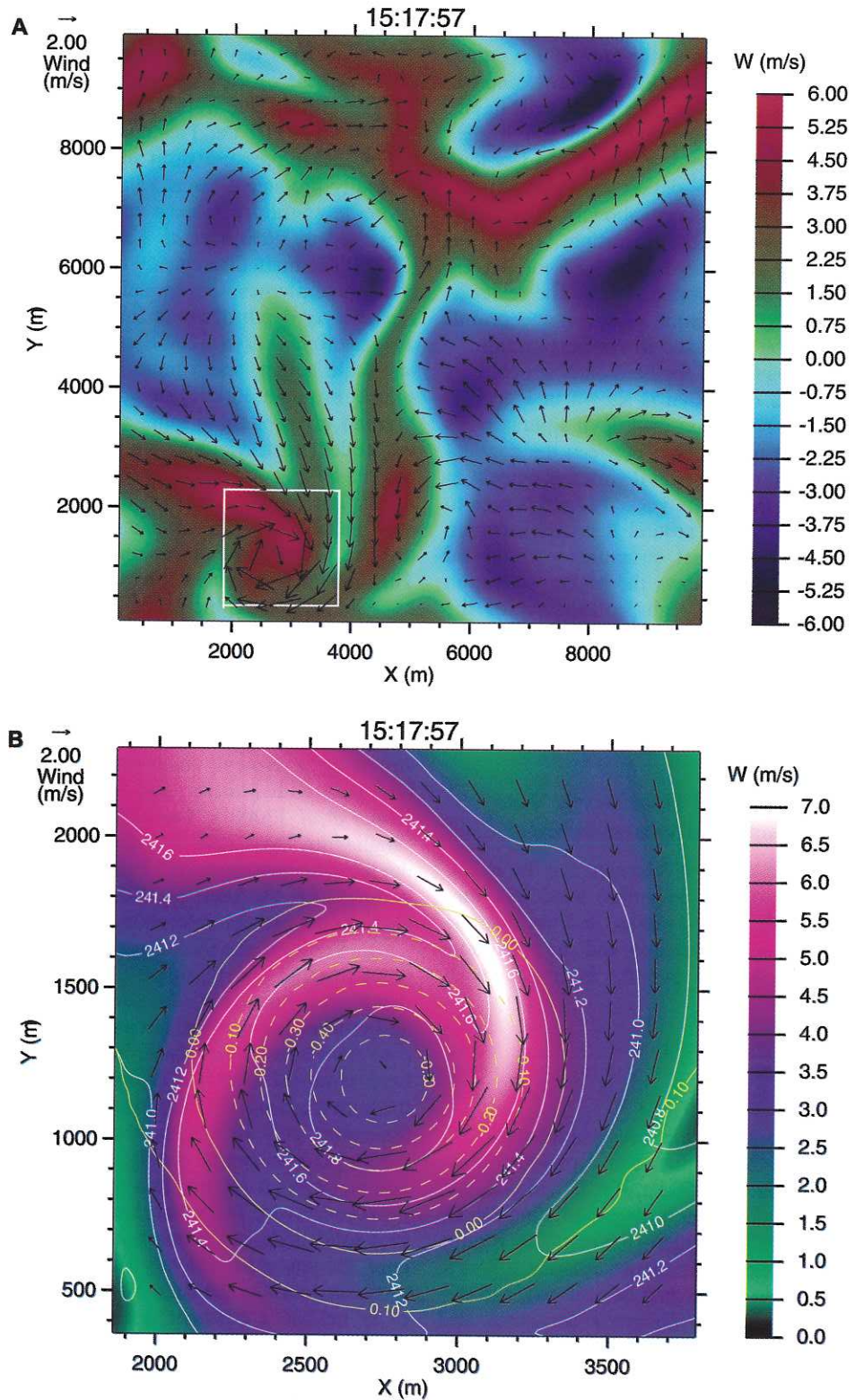


**Figure 5.** Plots of the “no wind” simulation dust devil at a height of 1.4 km above the surface in both (a) the base-resolution case, and (b) in the high-resolution case. Plots show upward velocity in m/s in the background color scale and the horizontal wind vector as black arrows. The white box in (a) represents the high-resolution region shown in (b). (b) also shows temperature at this level in K in white contours, and pressure perturbation at this level in Pa is plotted in yellow contours.

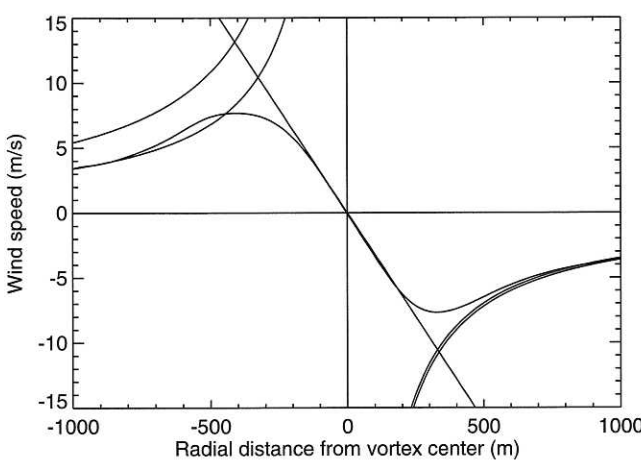


**Figure 6.** Comparison of the “no wind” simulation dust devil with a Rankine vortex. Tangential wind speeds as a function of distance from the dust devil center are plotted along with idealizations of speed versus distance from a Rankine vortex. The straight line near the center is speed equals a constant times radial distance. Two curved line fits of  $v = C/r$  (where  $C$  is a constant) have been drawn. The first is a fit to the wind speed at farthest distance from the vortex core. The second is a fit so that it will intersect the “solid body rotation”-type curve ( $v_r = \text{constant}$ ) at the same place that the modeled vortex shows a maximum in tangential wind speed.

observed terrestrial dust devils, and laboratory vortex flows [Sinclair, 1973].

[31] Dust devils have been observed in orbiter images of Mars, as well as from landers [Malin and Edgett, 2001; Cantor et al., 2002; Fisher et al., submitted manuscript, 2002]. Dust devils have been observed in both the wide angle and narrow angle cameras on Mars Global Surveyor. The highest resolution images generated by the wide-angle images have 250 m pixels, and have been able to resolve dust devils at many different sites. These images suggest the visible portion of dust devils can be 0.5 to 1 km in diameter and several kilometers high. These dimensions suggest that the dust devil simulated in the two LES cases are roughly consistent with observed structures. A more detailed assessment of dust devil occurrence and size is presented by Fisher et al. (submitted manuscript, 2002).

## 8. Dust Devil Budgets of Energy and Vorticity

[32] The modeled turbulent kinetic energy (TKE: the amount of kinetic energy in the perturbation wind field; in this paper, the perturbation is calculated with respect to a mean over the whole computational domain) is concentrated within the convective boundary layer, as expected [Stull, 1988]. For a region containing the “no wind” LES case dust devil, the TKE remains nearly constant. The only trend of any note within such a region is the redistribution of TKE to higher levels as the vortex passes into the domain. The time rate of change of TKE can be written [Stull, 1988, equation (5.1a)]

$$\frac{D\bar{e}}{Dt} = \delta_{B3} \frac{g}{\theta} (\bar{u}'_i \theta') - \bar{u}'_i \bar{u}'_j \frac{\partial \bar{U}_i}{\partial x_j} - \frac{\partial (\bar{u}'_i e)}{\partial x_i} - \frac{1}{\bar{\rho}} \frac{\partial (\bar{u}'_i p')}{\partial x_i} - \varepsilon \quad (2)$$

where  $\bar{e}$  is the turbulent kinetic energy ( $\bar{e} = \sum_{i=1}^3 (\bar{u}'_i)^2$ ,  $\bar{u}'_i = u_i - \bar{U}_i$ ), the first term on the right hand side is the buoyancy production ( $\delta_{ij}$  is the Kronecker delta,  $\theta$  is potential temperature, and  $g$  is the acceleration due to gravity), the second term is shear generation, the third term is turbulent transport, the fourth term is pressure correlation, and the fifth term is dissipation. Using the LES, a sixth term comes into play, which is generation of TKE by sub-grid-scale motions (buoyancy and/or shear). As described in section 2, the sub-grid-scale diffusion is nonzero as the model still has finite resolution and some diffusivity is specified at each model level throughout the domain.

[33] The components to the TKE equation, which sum nearly to zero, are shown in Figure 7. The buoyancy term is significantly stronger than the shear generation term throughout the domain, confirming the nature of the convection as free, as opposed to forced, consistent with weak horizontal winds and strong vertical thermal contrast. The resolved buoyancy generation peaks in the mid-boundary layer, at a height where there is optimal product of upward perturbation motions (which increase with height, as the buoyancy has chance to accelerate them) and positive perturbation of potential temperature (which decreases away from the surface and the energetic source of the buoyancy). Turbulent transport is strongly negative in the lower boundary layer, switching to strongly positive in the upper boundary layer. This represents turbulent transport of TKE out of the region of strong TKE and upward into the region of weak TKE. Dissipation by sub-grid-scale motions balances the majority of the TKE generation at upper levels by turbulent transport. At lower levels, the loss of TKE to transport is balanced by buoyancy generation, and (to a lesser degree) by generation of TKE by sub-grid-scale processes. Sub-grid-scale diffusion in this case is effectively simulating buoyancy generation in the lower PBL where the resolved vertical velocities have not yet grown large enough. It seems possible that this may reflect excessive sub-grid-scale vertical diffusivity, but tests with diffusivity

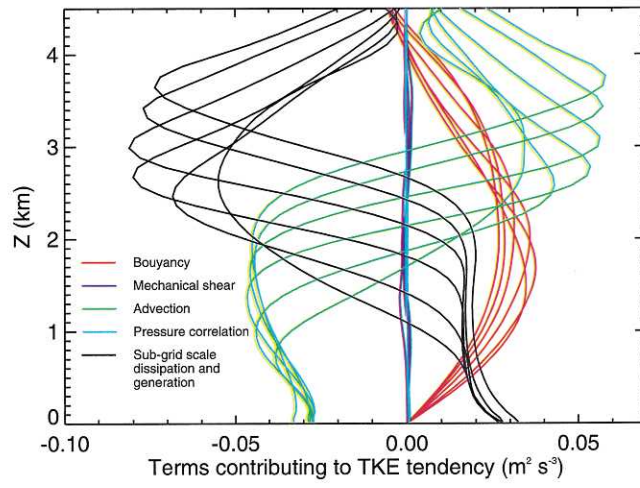


**Figure 7.** Magnitude of terms in the turbulent kinetic energy (TKE) budget for the “no wind” case simulation. Six lines are shown for each term, representing an instant in the development of the dust devil. The six instants span the time bracketed by the times shown in Figures 2c and 2d.

further reduced yielded terminal instability. These sub-grid-scale generation processes correspond to the model's surface and boundary layer diffusion scheme vertically mixing heat and momentum. The dust devil is therefore driven primarily by buoyancy (it is a buoyant, convective plume), with turbulent transport processes acting to vertically smooth the TKE distribution. Small-scale dissipative processes act to reduce the TKE.

[34] The origin of dust devil vorticity is somewhat more enigmatic than that of the energy. Does the dust devil simply concentrate vorticity from the surrounding environment? Alternatively, is it extracted from twisting of horizontal vorticity? (Note that we use the terms "twisting" and "tilting" interchangeably to describe the rotation of the three-dimensional vorticity vector out of one plane and into another.) The generation of a dust devil in a LES simulation with no initial wind or wind shear suggests that environmental vorticity is not the ultimate or primary vorticity source. This result is also supported by the zero wind LES case run by *Kanak et al.* [2000]. Examination of the three-dimensional vorticity equation, which is derived by taking the curl of the three-dimensional, nonhydrostatic momentum equations (neglecting planetary vorticity and viscous friction), yields some insight into ultimate sources of vorticity for the dust devil:

$$\frac{D\vec{\zeta}}{Dt} = -(\vec{\nabla} \cdot \vec{v})\vec{\zeta} + (\vec{\zeta} \cdot \vec{\nabla})\vec{v} + \frac{R}{P}(\vec{\nabla}P \times \vec{\nabla}T) \quad (3)$$

where  $\vec{\zeta}$  is the three-dimensional vorticity vector ( $\vec{\zeta} \equiv \vec{\nabla} \times \vec{v}$ ), R is the gas constant, P is the pressure, and T is the temperature. (For a more complete derivation, see *Pedlosky* [1987, chap. 2].) The three terms on the right hand side represent, respectively, the vorticity divergence (negative vorticity concentration), twisting of vorticity from one direction into another (allowing coupling between vorticity fields in different directions), and the solenoidal term that allows vorticity generation through pressure and temperature gradients (for example, temperature gradients between land and sea allow for horizontal vorticity generation, resulting in the widely known "sea-breeze" circulation).

[35] Examining our "no wind" LES case, there is initially no vorticity in any direction. The vorticity equation has no inherent preferred direction for vorticity generation. However, examination of the solenoidal term shows that in a planetary atmosphere, there is a strong preference for horizontal vorticity generation over a heated surface due to the fact that the solenoidal term is substantially larger in the vertical direction (where its magnitude is roughly  $\rho g$ ) than in the horizontal directions. As the surface warms after dawn, the vertical potential temperature structure becomes unstable. Small perturbations in the horizontal direction will grow, yielding a horizontal temperature gradient that couples strongly with the vertical pressure gradient, generating horizontal vorticity in the form of horizontal convective rolls. Vertical vorticity is substantially harder to generate from the solenoidal term due to weak horizontal pressure gradients (1 to 2 orders of magnitude lower than in the vertical even for the well-developed dust devils simulated in this study). As the flow becomes turbulent, however, substantial spatial heterogeneity develops in the perturbation wind field, allowing the twisting term to pump the

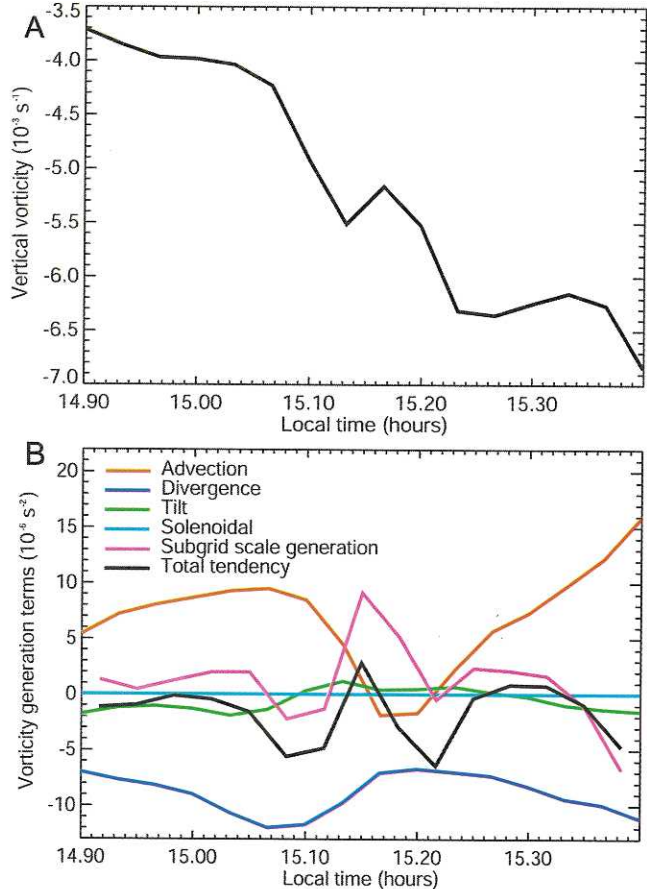


**Figure 8.** (a) Vertical component of vorticity as a function of time for the "no wind" case dust devil. Vorticity shown is an average over a box centered on the dust devil vorticity extremum, approximately 2 km on a side and about 3 km in height. The time span is the same as that shown in Figure 2. The dust devil generally increases in negative vorticity with time. (b) The different components of the vertical vorticity equation, showing terms contributing to the generation of vorticity. At this time in the dust devil's life, the two major terms come from advection of negative vorticity away from the dust devil, and the intensification of negative vorticity by convergence of winds.

buoyantly generated horizontal vorticity into the vertical direction.

[36] The origin of vertical vorticity in the planetary boundary layer is a more general issue from that of the origin of vorticity in the dust devil. Figure 8a shows the trend in vertical vorticity within the region of the "no wind" LES case within which the strong dust devil develops. The plot covers the period illustrated in Figure 2. Vertical vorticity decreases strongly during the period, as the dust devil spins up. The terms contributing to the vorticity tendency are shown in Figure 8b. The total tendency, throughout the majority of the study period, results from a slight under-compensation of the vorticity divergence by the advection of vorticity. Tilting of vorticity is not seen to be a major component of the vorticity tendency, despite previous suggestions that this may be the predominant dust devil formation term [*Maxworthy*, 1973; *Kanak et al.*, 2000]. Generation of vertical vorticity directly

from pressure and temperature gradients in the horizontal is seen to be inconsequential.

## 9. Summary and Conclusions

[37] This study has focused on examining the origin and nature of dust devils using a very high-resolution, three-dimensional numerical model. Four simulations, at 100 m horizontal resolution, were undertaken with differing initial wind fields. Dust devils have been found to develop in two of these cases: with no initial wind, and with maximum initial wind and shear. On the basis of this admittedly limited statistical sampling, we propose that dust devil development is not strongly sensitive to background wind speed or shear. The development of a dust devil in the no wind case also suggests that vorticity need not be present in the mean wind field. This result likely reflects the ability of the planetary boundary to rapidly develop horizontal vorticity as a result of free convection, followed by the generation of vertical vorticity by turbulent twisting of the vorticity field. The proximate development of dust devils, however, does appear to result primarily from the convergence of environmental vertical vorticity into the plume. The role of vorticity tilting seems to be in providing the environment with the necessary population of vertical vorticity extrema, rather than in the direct generation of the dust devil vortices. Consideration of the turbulence kinetic energy equation terms suggests that turbulence and convection in the planetary boundary layer is driven predominantly by buoyancy, and that the dust devils developed in the simulations can be considered rotating, free-convective plumes.

[38] The two dust devils that develop in the LES simulations are clearly distinct from other rotating and non-rotating plumes. The time trend of maximum and minimum domain vorticity (Figure 1) shows vorticity peaks associated with the dust devils that are a factor of 2 to 3 greater than observed in the absence of dust devils. When map projected, the vorticity field shows the development of sharp, nearly circular structures. Winds in the vortex walls and the central pressure drop confirm that the vortices are in cyclostrophic balance. The tangential velocity distribution is close to that of a Rankine vortex, which has been shown to explain the velocity distribution in terrestrial dust devils and laboratory fluid vortices. Vertical cross sections through the vortices show a structure with strong upward motion in the vortex walls with much decreased vertical motion in the core. Within the lowest few tens of meters, the central motion is actually downward, providing a first numerical simulation of this aspect of field observations by Sinclair [1973]. These detailed aspects of the modeled dust devil structure are very clearly illustrated in a nested 10 m-resolution domain, centered on the “no wind” case dust devil. While the high-resolution simulation allowed more detail to emerge in the vortex, it did not yield major differences in vortex radius, central pressure drop, or peak tangential winds. This is in accordance with a cyclostrophically balanced vortex and with the thermodynamic scaling relationships for dust devils developed by Renno *et al.* [1998].

[39] Although we use the term “dust devil” in this paper, the convective vortices may not have lifted dust. The

surficial wind stresses in the dust devils simulated in this paper were below laboratory measured threshold values for linear flow. However, since the mechanisms by which dust is lifted from the Martian surface are far from well understood (stress-initiated saltation, pressure drop, electrostatic charging, etc.), it is not clear that the simulated dust devils would not have lifted dust. Despite this uncertainty, we feel confident in using the term as the structures developed in this paper agree very well with theory (quantitatively) and observations (qualitatively) of dust devils, and the simulated vortices are clearly distinct from other structures developed in the model PBL (they are not simply the largest of a continuum of similar structures, as clearly illustrated in Figures 1 and 2). Comparison of the central pressure drop with those observed for Martian dust devils by the Mars Pathfinder (tabulated by Renno *et al.* [2000] and Murphy and Nelli [2002]), suggests the simulated dust devils are of a similar size to the smallest of the observed structures. The MPF observations further suggest that a vortex with a pressure drop just twice that of our predicted vortex was accompanied by a drop in solar power generation [Golombek *et al.*, 1999], consistent with a dust-populated vortex wall. Future LES experiments will concentrate on attempts to develop more vigorous dust devils, by increasing the surface-atmosphere temperature contrast and by increasing surface drag. It will also be interesting to trace dust lifting within the vortex structure, using both the model’s Eulerian dust transport model [Toigo and Richardson, 2002], and an off-line Lagrangian tracer scheme [Eluszkiewicz *et al.*, 1995]. Assessment of the dust lifting capacity by dust devils, and the dependencies should be of significant value in understanding the Martian dust cycle, both directly and through generation of parameterizations for use in lower-resolution, regional (mesoscale) and global (general circulation) models.

[40] **Acknowledgments.** We would like to thank two anonymous reviewers for their help in improving the manuscript. This work was supported by NASA Grant NAG5-10579 as part of the Mars Data Analysis Program.

## References

- Cantor, B., M. Malin, and K. S. Edgett, Multiyear Mars Orbiter Camera (MOC) observations of repeated Martian weather phenomena during the northern summer season, *J. Geophys. Res.*, **107**(E3), 5014, doi:10.1029/2001JE001588, 2002.
- Dudhia, J., A nonhydrostatic version of the Penn State-NCAR mesoscale model: Validation tests and simulation of an Atlantic cyclone and cold front, *Mon. Weather Rev.*, **121**, 1493–1513, 1993.
- Eluszkiewicz, J., R. A. Plumb, and N. Nakamura, Dynamics of wintertime stratospheric transport in the Geophysical Fluid Dynamics Laboratory SKYHI general circulation model, *J. Geophys. Res.*, **100**, 20,883–20,900, 1995.
- Golombek, M. P., et al., Overview of the Mars Pathfinder Mission: Launch through landing, surface operations, data sets, and science results, *J. Geophys. Res.*, **104**, 8523–8553, 1999.
- Greeley, R., N. Lancaster, S. Lee, and P. Thomas, Martian aeolian process, sediments and features, in *Mars*, edited by H. H. Kieffer *et al.*, pp. 730–766, Univ. of Ariz. Press, Tucson, 1992.
- Hong, S.-Y., and H.-L. Pan, Nonlocal boundary layer vertical diffusion in a medium-range forecast model, *Mon. Weather Rev.*, **124**, 2322–2339, 1996.
- Kanak, K. M., D. Lilly, and J. Snow, The formation of vertical vortices in the convective boundary layer, *Q. J. R. Meteorol. Soc.*, **126**, 2789–2810, 2000.
- Liu, J., M. I. Richardson, and R. J. Wilson, An assessment of the global, seasonal, and interannual spacecraft record of Martian climate in the thermal infrared, *J. Geophys. Res.*, **108**, doi:10.1029/2002JE001921, in press, 2003.

- Malin, M. C., and K. S. Edgett, Mars Global Surveyor Mars Orbiter Camera: Interplanetary cruise through primary mission, *J. Geophys. Res.*, **106**, 23,429–23,570, 2001.
- Maxworthy, T., Vorticity source for large-scale dust devils and other comments on naturally occurring columnar vortices, *J. Atmos. Sci.*, **30**, 1717–1722, 1973.
- Metzger, S. M., J. R. Carr, J. R. Johnson, T. J. Parker, and M. T. Lemmon, Dust devil vortices seen by the Mars Pathfinder camera, *Geophys. Res. Lett.*, **26**, 2781–2784, 1999.
- Murphy, J. R., and S. Nelli, Mars Pathfinder convective vortices: Frequency of occurrence, *Geophys. Res. Lett.*, **29**(23), 2103, doi:10.1029/2002GL015214, 2002.
- Pedlosky, J., *Geophysical Fluid Dynamics*, Springer-Verlag, New York, 1987.
- Rafkin, S., R. Haberle, and T. Michaels, The Mars regional atmospheric modeling system: Model description and selected simulations, *Icarus*, **151**, 228–256, 2001.
- Renno, N. O., M. L. Burkett, and M. P. Larkin, A simple thermodynamical theory for dust devils, *J. Atmos. Sci.*, **55**, 3244–3252, 1998.
- Renno, N. O., A. A. Nash, J. Lunine, and J. Murphy, Martian and terrestrial dust devils: Test of a scaling theory using Pathfinder data, *J. Geophys. Res.*, **105**, 1859–1865, 2000.
- Ryan, J. A., and J. J. Carroll, Dust devil wind velocities—Mature state, *J. Geophys. Res.*, **75**, 531–541, 1970.
- Ryan, J. A., and R. D. Lucich, Possible dust devils, vortices on Mars, *J. Geophys. Res.*, **88**, 11,005–11,011, 1983.
- Schofield, J. T., J. R. Barnes, D. Crisp, R. M. Haberle, S. Larsen, J. A. Magalhães, J. R. Murphy, A. Seiff, and G. Wilson, The Mars Pathfinder Atmospheric Structure Investigation/Meteorology (ASI/MET) Experiment, *Science*, **278**, 1752–1758, 1997.
- Sinclair, P. C., General characteristics of dust devils, *J. Appl. Meteorol.*, **8**, 32–45, 1969.
- Sinclair, P. C., Lower structure of dust devils, *J. Atmos. Sci.*, **30**, 1599–1619, 1973.
- Stull, R. B., *An Introduction to Boundary Layer Meteorology*, Kluwer Acad., Norwell, Mass., 1988.
- Thomas, P., and P. J. Gierasch, Dust devils on Mars, *Science*, **230**, 175–177, 1985.
- Toigo, A. D., and M. I. Richardson, A mesoscale model for the Martian atmosphere, *J. Geophys. Res.*, **107**(E7), 5049, doi:10.1029/2000JE001489, 2002.
- Toigo, A. D., M. I. Richardson, R. J. Wilson, H. Wang, and A. P. Ingersoll, A first look at dust lifting and dust storms near the south pole of Mars with a mesoscale model, *J. Geophys. Res.*, **107**(E7), 5050, doi:10.1029/2001JE001592, 2002.
- Webb, E. K., Temperature and humidity structure in the lower atmosphere, in *Geodetic Refraction: Effects of Electromagnetic Wave Propagation Through the Atmosphere*, edited by F. K. Brunner, pp. 85–141, Springer-Verlag, New York, 1984.
- Willis, G. E., and J. Deardorff, Laboratory observations of turbulent penetrative convection planforms, *J. Geophys. Res.*, **84**, 296–301, 1979.
- Young, G. S., D. A. R. Kristovich, M. R. Hjelmfelt, and R. C. Foster, Rolls, streets, waves, and more—A review of quasi-two-dimensional structures in the atmospheric boundary layer, *Bull. Am. Meteorol. Soc.*, **83**, 997–1001, 2002.
- Zurek, R. W., J. R. Barnes, R. M. Haberle, J. B. Pollack, J. E. Tillman, and C. B. Leovy, Dynamics of the atmosphere of Mars, in *Mars*, edited by H. H. Kieffer et al., pp. 835–933, Univ. of Ariz. Press, Tucson, 1992.

---

S. P. Ewald and M. I. Richardson, Division of Geological and Planetary Sciences, MS 150-21, California Institute of Technology, Pasadena, CA 91125, USA.

P. J. Gierasch and A. D. Toigo, Cornell University, Ithaca, NY 14853, USA. (toigo@astro.cornell.edu)